Phase-Resolved Functional Lung (PREFUL) MRI: The Next-Generation Ventilation-Perfusion Scan?

Andreas Voskrebenzev, Ph.D.[1,2,3]; Filip Klimeš, Ph.D.[1,2,3]; Jens Vogel-Claussen, M.D.[1,2,3]

[1]Institute for Diagnostic and Interventional Radiology, Hannover Medical School, Hannover, Germany
[2]Biomedical Research in End-Stage and Obstructive Lung Disease (BREATH), Member of the German Center for Lung Research (DZL), Hannover, Germany
[3]BioVisioneers GmbH, Laatzen, Germany

Introduction

Chronic pulmonary diseases – such as chronic obstructive pulmonary disease (COPD), cystic fibrosis (CF), and chronic thromboembolic pulmonary hypertension (CTEPH) – require accurate and sensitive diagnostic techniques to monitor progression and therapeutic response [1]. Traditional pulmonary function tests (PFTs), including the Tiffeneau-Pinelli index, provide global lung function parameters but lack the capacity to map region-specific changes [2]. Imaging approaches like computed tomography (CT) or single photon emission computed tomography (SPECT) can visualize lung morphology and function but inevitably involve ionizing radiation, making repeated examinations challenging [3, 4].

Magnetic resonance imaging (MRI) offers a promising, radiation-free alternative for lung function assessment. Although low proton density and rapid signal decay in the lung pose technical challenges [5], several methods have been developed to address these limitations. For instance, fluorinated ^{19}F or hyperpolarized gas MRI (e.g., ^{129}Xe) provides direct ventilation imaging [6] and, when paired with intravenous contrast [7], yields perfusion information. However, such techniques require specialized equipment, trained personnel, and contrast agents, and they may raise concerns over long-term safety.

Fourier decomposition (FD) is a contrast-free approach that uses conventional proton MRI and postprocessing to derive ventilation (V) and perfusion (Q) maps [8]. After image registration, the respiratory and cardiac frequency components of the time-series signal in each voxel are extracted, enabling simultaneous V/Q assessment. Soon, advanced versions of FD were developed [9–11], including self-gated non-contrast-enhanced functional lung imaging (SENCEFUL) [12]. Incorporating an additional DC acquisition in a quasi-random fast low-angle shot (FLASH) sequence allowed to sort each individual *k*-space line into one synthetic respiratory and cardiac cycle for higher temporal resolution and analysis of ventilation perfusion dynamics.

Following this idea, phase-resolved functional lung (PREFUL) MRI uses extended post-processing, allowing for retrospective image sorting according to respiratory and cardiac phases in combination with a conventional unmodified spoiled gradient-echo (GRE) or balanced steady state free precession (bSSFP) acquired in free breathing [13]. This allows dynamic V/Q assessment with commercially available sequences. Consequently, PREFUL MRI permits region-specific evaluations of dynamic lung function, including ventilation, perfusion, and even phase-based parameters such as flow-volume loop correlation metric (FVL-CM) [14] and pulse wave transit time or velocity measurements [15, 16]. Furthermore, many clinical studies have shown robust correlations with conventional methods [17–19, 15], reproducibility across different centers [20–22], and sensitivity in therapeutic and monitoring situations [23–29].

Despite these promising results, PREFUL remains restricted to a few specialized centers, partly due to limited awareness of the method's technical feasibility and clinical potential. This work aims to provide an overview of the current PREFUL methodology, thereby facilitating broader implementation.

Theory

Four main components – proton density, time-of-flight (TOF) effects, movement, and noise – primarily influence the pulmonary time-series MR signal in free-breathing spoiled gradient-echo acquisitions. Additional factors (e.g., T1, T2/T2* decay, diffusion, field inhomogeneities) are typically minimized through appropriate protocols (low flip angle, short TR, asymmetric echo, and dynamic parallel imaging [30]) and thus are omitted here. Pulmonary and cardiac motion during the MR acquisition is compensated by image registration. During expiration, shrinking lung volume increases proton density and thus raises the MR signal; during inspiration, the opposite occurs, forming the basis of ventilation measurements through the signal-volume relationship [31, 32]:

Equation 1

$$S \sim 1 / V$$

Pulsatile blood inflow induces further signal modulations known as TOF effect, which underpin perfusion measurements. Given the lung's inherently low signal, averaging and filtering improve signal-to-noise ratio so that the remaining variations predominantly reflect ventilation and perfusion. Because these variations occupy distinct frequency ranges, they can be separated by Fourier analysis [33]. Ventilation is then quantified via the inverse relationship between lung volume and proton signal, yielding the regional ventilation (RVent) [34] parameter:

Equation 2

$$RVent = \frac{V_{Insp} - V_{Exp}}{V_{Reg}} = \frac{S_{Reg}}{S_{Insp}} - \frac{S_{Reg}}{S_{Exp}}$$

During the initial transient phase of the acquisition, the MR signal has not yet reached steady state (SS) and thus briefly reflects near-maximal magnetization. By fitting these early

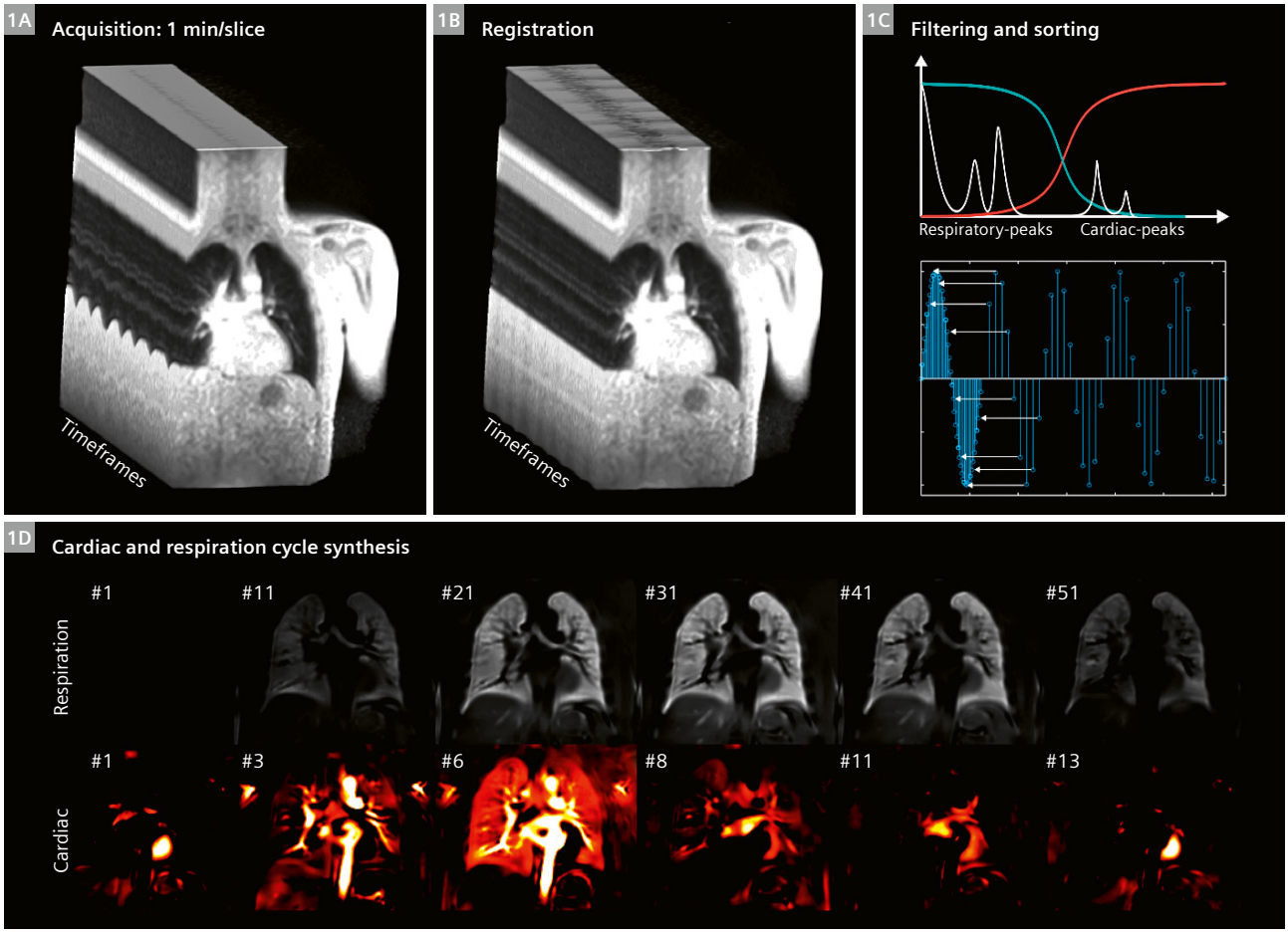

1 Simplified illustration of the phase-resolved functional lung (PREFUL)[1] MRI workflow: **(1A)** Free-breathing spoiled gradient-echo acquisition, **(1B)** motion correction via image registration, **(1C)** signal filtering (high-pass (red curve) and low-pass (blue curve)) and phase sorting, and **(1D)** synthesis of the cardiac and respiratory cycles (subset of phases provided). The resulting data are then quantified to yield various functional parameters and generate a final report.

data points to an exponential curve, it is possible to estimate the maximum signal (S_0). In addition, the signal drop between S_0 and steady state captures the potential effect if all voxels were moving. Together, these measurements serve as normalization factors for blood fraction (BF) content:

Equation 3

$$BF = S_{0,Map} / S_{0,Vessel}$$

and for flow-related signal difference Q in the steady state:

Equation 4

$$EF = Q / Median\ (S_0 - SS)$$

as fully detailed by Glandorf et al. [35], and allow full quantification of perfusion (QQ) in mL/min/100 mL:

Equation 5

$$QQ = EF \cdot BF \cdot VV \cdot f_{Heart} \cdot \frac{60\ s}{min} \cdot \frac{100}{VV \cdot 100}$$

with the heart frequency f_{Heart} determined from the fourier spectrum and the voxel volume (VV).

Methods

Figure 1 gives a simplified overview of the core protocol steps, consisting of acquisition, registration, filtering and sorting, and final cycle synthesis. Further details are described in the following sections. More in-depth information can be found in previous articles [13, 36].

For this article, retrospective evaluation of unpublished data from a healthy volunteer and a representative CF patient who participated in a previously published study on elexacaftor-tezacaftor-ivacaftor (ETI) therapy [28] was performed.

Acquisition

After standard MRI safety precautions and prescreening for contraindications, participants are placed head-first and supine on a 0.55T, 1.5T, or 3T scanner table. A multi-channel flex coil is positioned beneath the chin to optimize signal coverage of the lungs, and care is taken to secure it without restricting breathing. Localizer scans establish orientation, and a transversal morphological image is acquired to identify the tracheal bifurcation, which serves as a consistent landmark for coronal slices. Depending on the protocol length, either a limited number of slices (e.g., three slices spaced at 100%) or multiple slices with smaller spacing (20%–33%) are acquired to cover the lungs; each slice is acquired separately rather than interleaved. Typical temporal resolutions range from approximately 3 to 5 images/second. A representative protocol is provided in Table 1. Example slice positioning is shown in Figure 2.

Parameter	Setting
Sequence	SPGRE, bSSFP
Orientation	Coronal
Field of view (FOV)	500 × 500 mm²
Slice thickness (ST)	15 mm
Repetition time (TR)	3 ms or lower
Echo time (TE)	1 ms or lower
Bandwidth (BW)	1500 Hz/Pixel
Flip angle (FA)	~5° (Ernst angle)
Acceleration	T-GRAPPA 2×
Temporal resolution (dt)	> 3 frames/second
Frames/measurements	up to 500 depending on dt
Total duration / slice	1 minute

Table 1: Typical sequence settings for a PREFUL[1] acquisition. Please note that some settings such as TE, TR, and FA will depend on the field strength and gradient system.

Postprocessing

Following acquisition, images are corrected for respiratory and cardiac motion, filtered for noise reduction and V/Q separation, and sorted to generate phase-resolved data for both ventilation and perfusion.

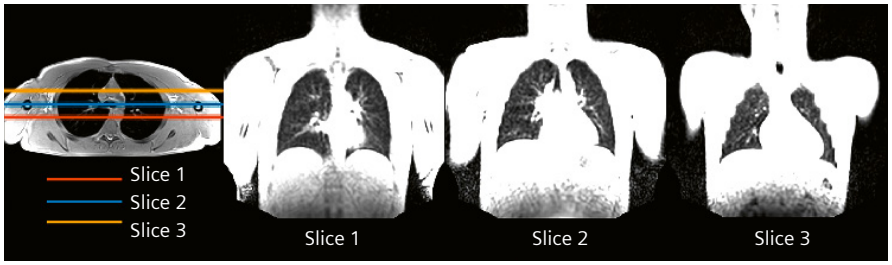

2 Example of slice positioning using a transverse volumetric interpolated breath-hold examination (VIBE) sequence for planning. Then, three coronal slices are acquired for PREFUL in free breathing with a 100% slice gap. The second slice is aligned with the tracheal bifurcation to serve as a repeatable anatomical landmark.

General segmentation
To enable a fully automated processing pipeline, all necessary segmentations are performed by either neural networks (nnU-Net/U-Net for lung boundaries [37] and vessel segmentation [38, 16]) or algorithmic methods for the large central vessel [18]. The final lung parenchyma region of interest (ROI) is then generated by subtracting the vessel segmentation from the lung boundary ROI. Figure 3 provides an illustration of the segmentation procedure.

Registration
Images are grouped into ten respiration-based categories (inspiration to expiration). Non-rigid registration is performed within each group toward an intermediate lung position, then progressively between groups until they converge to a mid-respiration reference (Group 5). This approach (GOREG) minimizes the deformation per registration step and enhances algorithmic stability [39]. As registration packages Advanced Normalization Tools (ANTs) [40] with BSplineSyN is known to deliver a good registration quality. However, the less-explored polynomial expansion-based algorithm ("Forsberg") [41, 42] can offer comparable results with shorter processing times [43, 44].

General filtering
Registered images are denoised using guided filtering [45] with the temporally averaged image as a guiding image. Low-pass and high-pass filters (cut-off around 0.7 Hz) are applied to separate perfusion- and ventilation-related components. The initial 20 images are discarded (except in quantified perfusion calculations) to ensure a steady-state signal.

Perfusion
Cardiac phase determination relies on algorithmically identifying strong perfusion-weighted signal regions in the lung and mediastinum (red ROI, Fig. 3) [18]. A piecewise sinusoidal fit of the corresponding time-series allows phase-sorting of the cardiac cycle, which is then interpolated (15 phases) to exceed the original sampling rate and generate high-temporal-resolution perfusion dynamics. This re-sorted dataset provides an entire cycle from diastole to systole, and back to diastole (Fig. 1).

Ventilation
Respiratory frequency and tidal volume can vary substantially, so a cosine model function is used to assign images to specific respiratory phases based on signal amplitude. The slope of the signal determines whether data belongs to inspiration or expiration. Nadaraya-Watson kernel regression then generates a uniformly sampled respiratory cycle. RVent is calculated by comparing the mid-respiration signal with inspiration and expiration signals (Equation 2) [34].

Parameter calculation and thresholding
The synthesized full cardiac and respiratory cycles enable derivation of additional functional parameters. RVent is computed at each phase, while FVL-CMs are calculated as an MRI analog to flow-volume loops of pulmonary function tests [14]. Quantified perfusion involves normalizing early transient-state images to account for proton density changes, fitting an exponential model to reach maximal magnetization, and then identifying cardiac phases with maximal lung parenchyma signal [46, 35]. Blood fraction and exchange fraction estimates are combined to calculate perfusion in mL/min/100 mL (Equation 5).

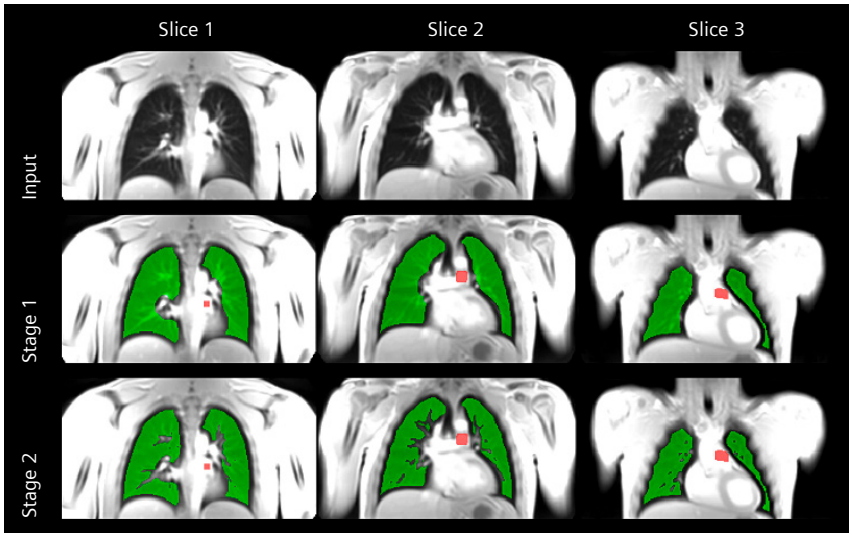

3 Illustration of the segmentation procedure for three slices. In the first stage, a neural network identifies the lung boundary (green). In the second stage, intraparenchymal vessels are excluded from the lung boundary. Separately, an algorithm segments a large vessel with a strong perfusion signal (red).

Parameter maps undergo static and dynamic thresholding to classify ventilation and perfusion defects (VD/QD). FVL-CM is thresholded with a fixed value of 90%. For the remaining parameters, the 90th percentile is used as an estimate for a normal value and multiplied with an empirical factor (0.4 for RVent and 0.15 for QQ).

Corresponding defect percentages are computed based on the proportion of voxels below the chosen thresholds relative to total lung parenchyma. Combining RVent and FVL-CM allows further subcategorization of V/Q defects according to a fourfold table (see Table 2).

Defect	VD	No VD
QD	VQM(D)	QDP(Ex)
No QD	VDP(Ex)	VQM(H)

Table 2: The resulting four combinations when comparing ventilation and perfusion defect (VD/QD): VQ match of defects (VQM(D)), VQ match of healthy regions (VQM(H)), and exclusive VDP and QDP.

All analyses in the results section use Forsberg registration and combine both RVent and FVL-CM metrics into a single VD measurement, classifying a voxel as VD if either RVent or FVL-CM (or both) met the defect criteria. Lung parenchyma parameters are summarized using mean values, and the complete set of ventilation/perfusion (V/Q) metrics is reported.

Results

Example data from a healthy volunteer (Fig. 4) demonstrate homogeneous ventilation and perfusion throughout the lung parenchyma, resulting in a 92% V/Q match. By contrast, a cystic fibrosis patient (Fig. 5) shows heterogeneous distribution before treatment, corresponding to a 40% V/Q match. Following therapy, all parameters improve markedly, culminating in a 93% V/Q match.

Discussion

In this article, we described the proton MRI technique known as PREFUL, providing example results to highlight its capabilities. A key distinction of PREFUL, compared to techniques like Fourier decomposition and its derivatives, is its combination with a conventional spoiled gradient echo (SPGRE) sequence. While balanced steady-state free precession (bSSFP) sequences deliver a signal-to-noise ratio advantage at 1.5T or lower, at 3T they suffer from reduced image quality and banding artifacts that hinder analysis [47]. Despite being developed for SPGRE, recent studies have demonstrated that PREFUL provides strong comparability with both sequences at 1.5T [48]. Besides the image sorting algorithm, as an additional major difference in post-processing, filtering is less restricted and amplitude calculation is carried out in time domain to account for frequency variations.

As outlined in the introduction, PREFUL has undergone validation against gold standards like SPECT, dynamic contrast-enhanced (DCE) MRI, and (hyperpolarized) gas MRI [49, 17, 18, 50, 19]. It has been tested in a variety of settings [51, 52, 20, 48, 44], including multi-center trials [21, 22, 53] and at 0.55T [25, 26, 54], demonstrating robust performance. PREFUL has proven capable of reflecting disease pathology and tracking disease progression and treatment responses [23, 55, 56, 24, 27, 57, 28, 16], making it a promising candidate for clinical translation. In particular, dynamic parameters like the spirometry-inspired FVL-CM have shown greater sensitivity as biomarkers compared to static measures that rely on only a limited portion of the synthesized cycles.

The main limitation of the PREFUL method lies in its coarse spatial resolution (4 × 4 × 15 mm^3) and moderate acquisition time (1 minute per 2D slice), which complicate detailed lung assessments. To address this, a 3D version of PREFUL has been developed, offering higher isotropic resolution (4 × 4 × 4 mm^3) and enabling more comprehensive ventilation dynamics measurements with a self-gated stack-of-stars VIBE or FLORET UTE sequence [58, 59] in about eight minutes. Despite being a relatively new technique, several studies have already validated the clinical applicability of 3D PREFUL [60, 43, 61]. However, a primary drawback of the 3D version is the lack of integrated perfusion information and the need for more specialized sequences. Consequently, 2D PREFUL remains a forward-looking technique, particularly as emerging biomarkers – such as pulse wave transit time or velocity measurements – gain traction. Ongoing advancements in image acceleration and protocol refinements may offer a near-term pathway to broader dissemination of the 2D PREFUL method.

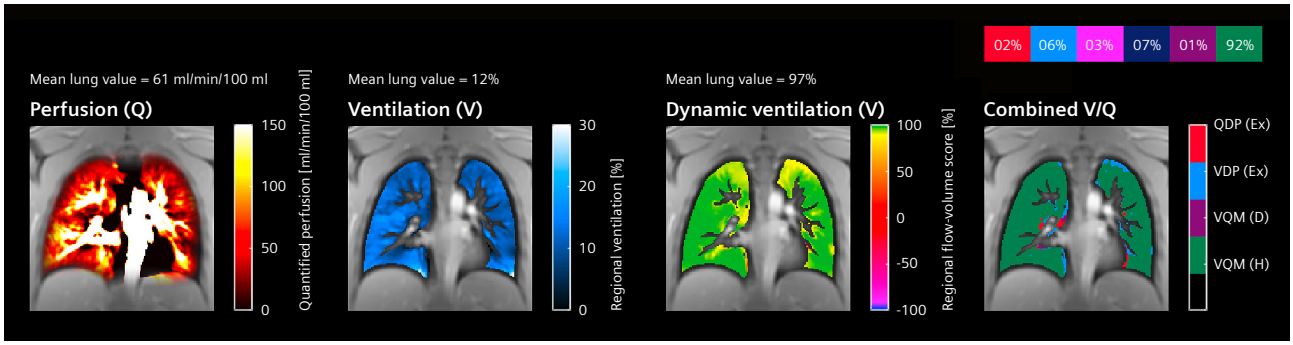

4 Example PREFUL maps of a healthy volunteer (male, age 36), showing perfusion in mL/min/100 mL, regional ventilation in %, flow-volume loop correlation metric (FVL-CM) in %, and a V/Q map obtained by thresholding and combining all maps. Please note the homogenous distribution of V/Q values in the lung parenchyma.

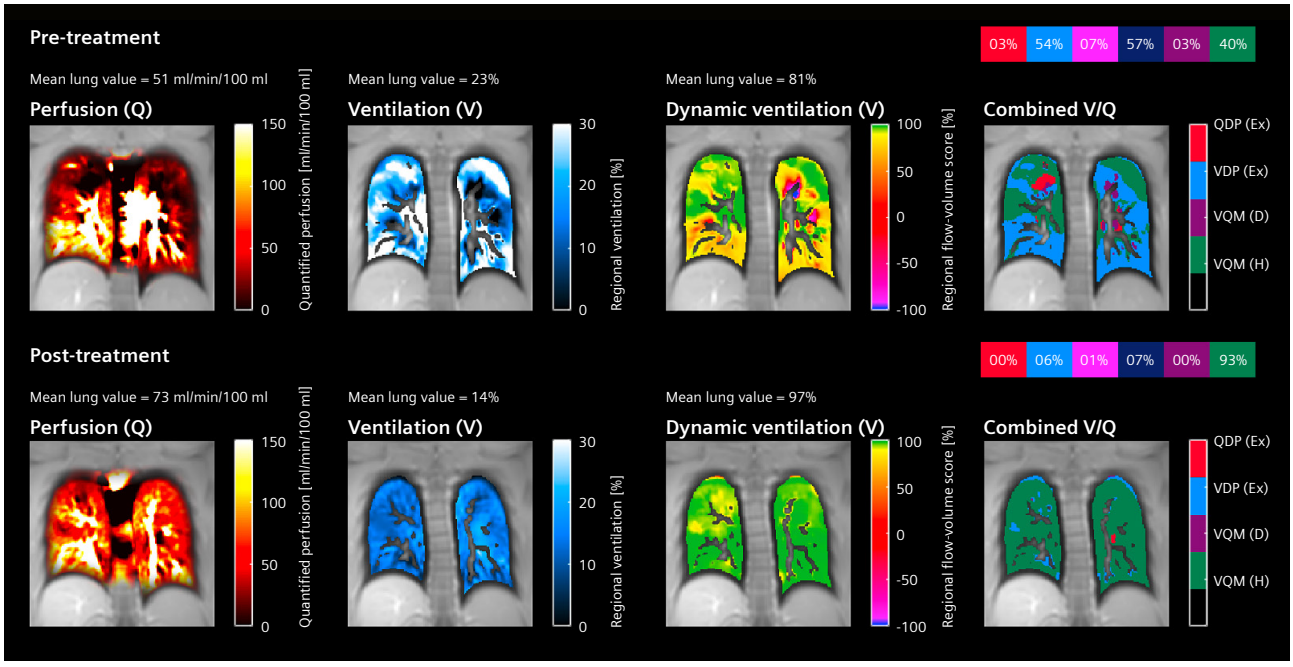

5 Pre- and post-treatment effect visualized for a CF patient (male, age 20) after ETI therapy. Please note the homogenization of V/Q after treatment, visible on all maps.

The LungMaps application from Siemens Healthineers

PREFUL technology will be available soon under the product name LungMaps[1] as a postprocessing application for MRI scanners from Siemens Healthineers. However, the nomenclature in the product is slightly different:

- RVent is called "Ventilation-weighted map" (Vw) without quantitative numbers.
- QQ is called "Perfusion-weighted map" (Qw) without quantitative numbers.
- FVL-CM is called "apparent flow volume loop correlation map" (aFVL).
- In the defect maps (see Table 2 and Figure 6), the product uses the following labels:
  – "Defect match" instead of VQM(D)
  – "Ventilation defect" instead of VDP(Ex)
  – "Perfusion defect" instead of QDP(Ex)
  – "No defect match" instead of VQM(H)

[1] *LungMaps is currently under development and not commercially available. Its future availability cannot be ensured.*

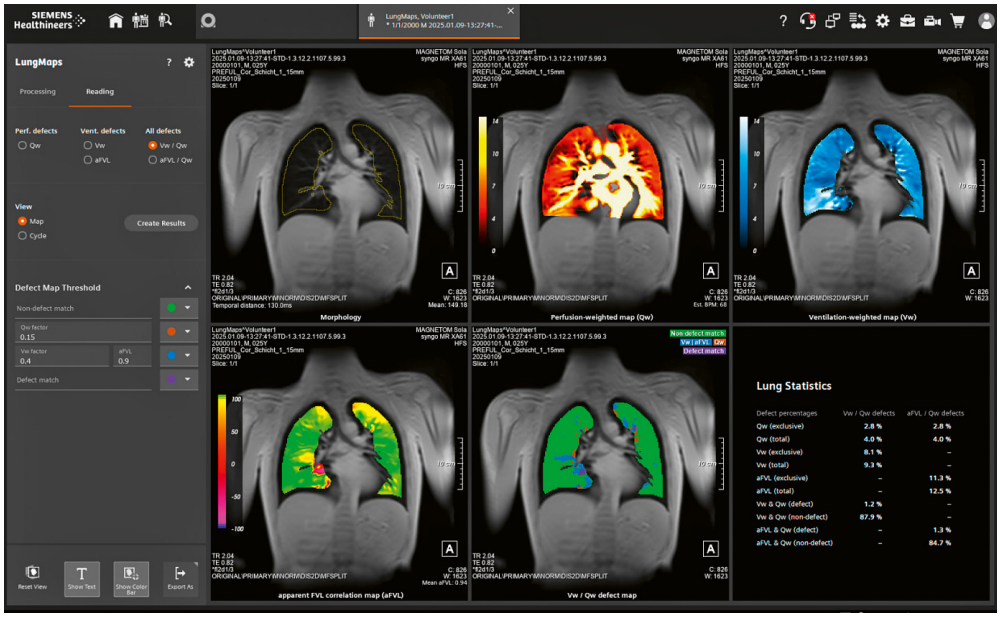

6 The LungMaps[1] application from Siemens Healthineers. This dataset from a healthy volunteer shows regular perfusion- and ventilation-weighted maps. The aFVL map and the Vw/Qw defect map show no signs of lung defects. The lower right corner displays a structured report of the defect percentages, which is also available as a PDF and as a secondary capture DICOM file.

To learn more about
LungMaps please visit us at

siemens-healthineers.com/magnetic-resonance-imaging/options-and-upgrades/clinical-applications/lungmaps

Figure 6 shows a screenshot of the application running on *syngo*.via, in this case on a healthy volunteer. All processing, including the neural network-based segmentation (see General segmentation) of the lungs and PREFUL analysis, is fully automated. However, the user can manually edit the lung segmentation if desired

Conclusion

PREFUL MRI provides a robust, radiation-free means of assessing ventilation and perfusion in a single free-breathing scan. Validation studies have consistently shown strong concordance with established methods like SPECT, DCE, and hyperpolarized gas MRI, underscoring its clinical potential. Although current 2D acquisitions use relatively coarse spatial resolution, the 3D version provides more detailed lung coverage, albeit without simultaneous perfusion and with less widespread sequences. Ongoing refinements in acquisition speed, resolution, and biomarker integration thus position 2D PREFUL as a promising candidate for next-generation V/Q scans using free-breathing proton-based pulmonary imaging.

References

1 Vogelmeier CF, Criner GJ, Martinez FJ, Anzueto A, Barnes PJ, Bourbeau J, et al. Global Strategy for the Diagnosis, Management, and Prevention of Chronic Obstructive Lung Disease 2017 Report: GOLD Executive Summary. Eur Respir J. 2017;49(3):1700214.
2 Ranu H, Wilde M, Madden B. Pulmonary Function Tests. Ulster Med J. 2011;80(2):84–90.
3 Galbán CJ, Han MK, Boes JL, Chughtai KA, Meyer CR, Johnson TD, et al. Computed tomography-based biomarker provides unique signature for diagnosis of COPD phenotypes and disease progression. Nat Med. 2012;18(11):1711–1715.
4 Roach PJ, Schembri GP, Bailey DL. V/Q Scanning Using SPECT and SPECT/CT. J Nucl Med. 2013;54(9):1588–1596.
5 Wild JM, Marshall H, Bock M, Schad LR, Jakob PM, Puderbach M, et al. MRI of the lung (1/3): methods. Insights Imaging. 2012;3(4):345–353.
6 Albert MS, Cates GD, Driehuys B, Happer W, Saam B, Jr CSS, Wishnia A. Biological magnetic resonance imaging using laser-polarized 129Xe. Nature. 1994;370(6486):199–201.
7 Berthezène Y, Vexler V, Clément O, Mühler A, Moseley ME, Brasch RC. Contrast-enhanced MR imaging of the lung: assessments of ventilation and perfusion. Radiology. 1992;183(3):667–672.
8 Bauman G, Puderbach M, Deimling M, Jellus V, Chefd'hotel C, Dinkel J, et al. Non-contrast-enhanced perfusion and ventilation assessment of the human lung by means of fourier decomposition in proton MRI. Magn Reson Med. 2009;62(3):656–664.

9 Bauman G, Bieri O. Matrix pencil decomposition of time-resolved proton MRI for robust and improved assessment of pulmonary ventilation and perfusion. Magn Reson Med. 2017;77(1):336–342.
10 Bondesson D, Schneider MJ, Gaass T, Kühn B, Bauman G, Dietrich O, et al. Nonuniform Fourier-decomposition MRI for ventilation- and perfusion-weighted imaging of the lung. Magn Reson Med. 2019;82(4):1312–1321.
11 Ilicak E, Ozdemir S, Schad LR, Weis M, Schoenberg SO, Zöllner FG, et al. Phase-cycled balanced SSFP imaging for non-contrast-enhanced functional lung imaging. Magn Reson Med. 2022;88(4):1764–1774. doi:10.1002/mrm.29302
12 Fischer A, Weick S, Ritter CO, Beer M, Wirth C, Hebestreit H, et al. SElf-gated Non-Contrast-Enhanced FUnctional Lung imaging (SENCEFUL) using a quasi-random fast low-angle shot (FLASH) sequence and proton MRI. NMR Biomed. 2014;27(8):907-917.
13 Voskrebenzev A, Gutberlet M, Klimeš F, Kaireit TF, Schönfeld C, Rotärmel A, et al. Feasibility of quantitative regional ventilation and perfusion mapping with phase-resolved functional lung (PREFUL) MRI in healthy volunteers and COPD, CTEPH, and CF patients. Magn Reson Med. 2018;79(4):2306–2314.
14 Voskrebenzev A, Klimeš F, Gutberlet M, Kaireit T, Schönfeld C, Renne J, et al. Imaging-Based Spirometry in Chronic Obstructive Pulmonary Disease (COPD) Patients using Phase Resolved Functional Lung Imaging (PREFUL). In: Proc Intl Soc Mag Reson Med. 26;2018:1079.
15 Pöhler GH, Löffler F, Klimeš F, Behrendt L, Voskrebenzev A, González CC, et al. Validation of Phase-Resolved Functional Lung (PREFUL) Magnetic Resonance Imaging Pulse Wave Transit Time Compared to Echocardiography in Chronic Obstructive Pulmonary Disease. J Magn Reson Imaging. 2022;56(2):605–615.
16 Wernz MM, Voskrebenzev A, Müller RA, Zubke M, Klimeš F, Glandorf J, et al. Feasibility, Repeatability, and Correlation to Lung Function of Phase-Resolved Functional Lung (PREFUL) MRI-derived Pulmonary Artery Pulse Wave Velocity Measurements. J Magn Reson Imaging. 2024;60(5):2216–2228. Epub March 9, 2024.
17 Kaireit TF, Voskrebenzev A, Gutberlet M, Freise J, Jobst B, Kauczor HU, et al. Comparison of quantitative regional perfusion-weighted phase resolved functional lung (PREFUL) MRI with dynamic gadolinium-enhanced regional pulmonary perfusion MRI in COPD patients. J Magn Reson Imaging. 2019;49(4):1122–1132.
18 Behrendt L, Voskrebenzev A, Klimeš F, Gutberlet M, Winther HB, Kaireit TF, et al. Validation of Automated Perfusion-Weighted Phase-Resolved Functional Lung (PREFUL)-MRI in Patients With Pulmonary Diseases. J Magn Reson Imaging. 2020;52(1):103–114.
19 Kaireit TF, Kern A, Voskrebenzev A, Pöhler GH, Klimes F, Behrendt L, et al. Flow Volume Loop and Regional Ventilation Assessment Using Phase-Resolved Functional Lung (PREFUL) MRI: Comparison With 129 Xenon Ventilation MRI and Lung Function Testing. J Magn Reson Imaging. 2021;53(4):1092–1105.
20 Pöhler GH, Klimeš F, Behrendt L, Voskrebenzev A, Gonzalez CC, Wacker F, et al. Repeatability of Phase-Resolved Functional Lung (PREFUL)-MRI Ventilation and Perfusion Parameters in Healthy Subjects and COPD Patients. J Magn Reson Imaging. 2021;53(3):915–927.
21 Behrendt L, Smith LJ, Voskrebenzev A, Klimeš F, Kaireit TF, Pöhler GH, et al. A dual center and dual vendor comparison study of automated perfusion-weighted phase-resolved functional lung magnetic resonance imaging with dynamic contrast-enhanced magnetic resonance imaging in patients with cystic fibrosis. Pulm Circ. 2022;12(2):e12054.
22 Marshall H, Voskrebenzev A, Smith LJ, Biancardi AM, Kern AL, Collier GJ, et al. 129Xe and Free-Breathing 1H Ventilation MRI in Patients With Cystic Fibrosis: A Dual-Center Study. J Magn Reson Imaging. 2023;57(6):1908–1921.
23 Alsady TM, Voskrebenzev A, Greer M, Becker L, Kaireit TF, Welte T, et al. MRI-derived regional flow-volume loop parameters detect early-stage chronic lung allograft dysfunction. J Magn Reson Imaging. 2019;50(6):1873–1882.
24 Voskrebenzev A, Kaireit TF, Klimeš F, Pöhler GH, Behrendt L, Biller H, et al. Pulmonary Dysfunction after Pediatric COVID-19. Radiology. 2023;306(3):e221250.
27 Vogel-Claussen J, Kaireit TF, Voskrebenzev A, Klimeš F, Glandorf J, Behrendt L, et al. Phase-resolved Functional Lung (PREFUL) MRI-derived Ventilation and Perfusion Parameters Predict Future Lung Transplant Loss. Radiology. 2023;307(4):e221958.
28 Dohna M, Voskrebenzev A, Klimeš F, Kaireit TF, Glandorf J, Pallenberg ST, et al. PREFUL MRI for Monitoring Perfusion and Ventilation Changes after Elexacaftor-Tezacaftor-Ivacaftor Therapy for Cystic Fibrosis: A Feasibility Study. Radiol Cardiothorac Imaging. 2024;6(2):e230104.
29 Ouyang T, Tang Y, Klimes F, Vogel-Claussen J, Voskrebenzev A, Yang Q. Phase-Resolved Functional Lung (PREFUL) MRI May Reveal Distinct Pulmonary Perfusion Defects in Postacute COVID-19 Syndrome: Sex, Hospitalization, and Dyspnea Heterogeneity. J Magn Reson Imaging. 2025;61(2):851–862. Epub June 17, 2024.
30 Breuer FA, Kellman P, Griswold MA, Jakob PM. Dynamic autocalibrated parallel imaging using temporal GRAPPA (TGRAPPA). Magn Reson Med. 2005;53(4):981–985.
31 Bankier AA, O'Donnell CR, Mai VM, Storey P, De Maertelaer V, Edelman RR, et al. Impact of lung volume on MR signal intensity changes of the lung parenchyma. J Magn Reson Imaging. 2004;20(6):961–966.
32 Zapke M, Topf HG, Zenker M, Kuth R, Deimling M, Kreisler P, et al. Magnetic resonance lung function – a breakthrough for lung imaging and functional assessment? A phantom study and clinical trial. Respir Res. 2006;7(1):106.
33 Deimling M, Jellus V, Geiger B, Chefd'hotel C. Time Resolved Lung Ventilation Imaging by Fourier Decomposition. Proc Intl Soc Mag Reson Med. 16; 2008:2639.
34 Klimeš F, Voskrebenzev A, Gutberlet M, Kern A, Behrendt L, Kaireit TF. Free-breathing quantification of regional ventilation derived by phase-resolved functional lung (PREFUL) MRI. NMR Biomed. 2019;32(6):e4088.
35 Glandorf J, Klimeš F, Behrendt L, Voskrebenzev A, Kaireit TF, Gutberlet M, et al. Perfusion quantification using voxel-wise proton density and median signal decay in PREFUL MRI. Magn Reson Med. 2021;86(3):1482–1493.
36 Voskrebenzev A, Klimeš F, Wacker F, Vogel-Claussen J. Phase-Resolved Functional Lung MRI for Pulmonary Ventilation and Perfusion (V/Q) Assessment. J Vis Exp. 2024;(210):e66380.
37 Isensee F, Jaeger PF, Kohl SAA, Petersen J, Maier-Hein KH. nnU-Net: a self-configuring method for deep learning-based biomedical image segmentation. Nat Methods. 2021;18(2):203–211.
38 Ronneberger O, Fischer P, Brox T. U-Net: Convolutional Networks for Biomedical Image Segmentation. In: Navab N, Hornegger J, Wells WM, Frangi AF, eds. Medical Image Computing and Computer-Assisted Intervention – MICCAI 2015. Lecture Notes in Computer Science. Springer Cham, Switzerland; 2015:234–241.
39 Voskrebenzev A, Gutberlet M, Kaireit TF, Wacker F, Vogel-Claussen J. Low-pass imaging of dynamic acquisitions (LIDA) with a group-oriented registration (GOREG) for proton MR imaging of lung ventilation. Magn Reson Med. 2017;78(4):1496–1505.

40 Avants BB, Tustison NJ, Song G, Cook PA, Klein A, Gee JC. A Reproducible Evaluation of ANTs Similarity Metric Performance in Brain Image Registration. Neuroimage. 2011;54(3):2033–2044.
41 Forsberg D, Andersson M, Knutsson H. Extending Image Registration Using Polynomial Expansion To Diffeomorphic Deformations. In: SSBA Symposium on Image Analysis. 2012:4.
42 Forsberg D. fordanic/image-registration. Published online 2022. Available at https://github.com/fordanic/image-registration. Accessed April 12, 2022.
43 Klimeš F, Voskrebenzev A, Gutberlet M, Grimm R, Wacker F, Vogel-Claussen J. Evaluation of image registration algorithms for 3D phase-resolved functional lung ventilation magnetic resonance imaging in healthy volunteers and chronic obstructive pulmonary disease patients. NMR Biomed. 2023;36(3):e4860.
44 Voskrebenzev A, Gutberlet M, Klimeš F, Kaireit TF, Shin HO, Kauczor HU, et al. A synthetic lung model (ASYLUM) for validation of functional lung imaging methods shows significant differences between signal-based and deformation-field-based ventilation measurements. Front Med (Lausanne). 2024;11:1418052.
45 He K, Sun J, Tang X. Guided Image Filtering. IEEE Trans Pattern Anal Mach Intell. 2013;35(6):1397-1409.
46 Behrendt L, Voskrebenzev A, Klimeš F, Gutberlet M, Winther HB, Kaireit TF, et al. Validation of Automated Perfusion-Weighted Phase-Resolved Functional Lung (PREFUL)-MRI in Patients With Pulmonary Diseases. J Magn Reson Imaging. 2020;52(1):103–114.
47 Bauman G, Pusterla O, Bieri O. Functional lung imaging with transient spoiled gradient echo. Magn Reson Med. 2019;81(3):1915–1923.
48 Hahn JJ, Voskrebenzev A, Behrendt L, Klimeš F, Pöhler GH, Wacker F, et al. Sequence comparison of spoiled gradient echo and balanced steady-state free precession for pulmonary free-breathing proton MRI in patients and healthy volunteers: Correspondence, repeatability, and validation with dynamic contrast-enhanced MRI. NMR Biomed. 2024;37(11):e5209. Epub July 12, 2024.
49 Marshall H, Voskrebenzev A, Biancardi A, Smith L, Tahir B, Wild J, et al. Comparison of 1H MRI and 3He MRI ventilation images in patients with cystic fibrosis and patients with lung cancer. Eur Respir J. 2018;52(suppl 62):PA387.
50 Couch MJ, Munidasa S, Rayment JH, Voskrebenzev A, Seethamraju RT, Vogel-Claussen J, et al. Comparison of Functional Free-Breathing Pulmonary 1H and Hyperpolarized 129Xe Magnetic Resonance Imaging in Pediatric Cystic Fibrosis. Acad Radiol. 2021;28(8):e209–e218.
51 Glandorf J, Klimeš F, Voskrebenzev A, Gutberlet M, Wacker F, Vogel-Claussen J. Effect of intravenously injected gadolinium-based contrast agents on functional lung parameters derived by PREFUL MRI. Magn Reson Med. 2020;83(3):1045–1054.
52 Glandorf J, Klimeš F, Voskrebenzev A, Gutberlet M, Behrendt L, Crisosto C, et al. Comparison of phase-resolved functional lung (PREFUL) MRI derived perfusion and ventilation parameters at 1.5T and 3T in healthy volunteers. PLOS ONE. 2020;15(12):e0244638.
53 Moher Alsady T, Voskrebenzev A, Behrendt L, Olsson K, Heußel CP, Gruenig E, et al. Multicenter Standardization of Phase-Resolved Functional Lung MRI in Patients With Suspected Chronic Thromboembolic Pulmonary Hypertension. J Magn Reson Imaging. 2024;59(6):1953–1964.
54 Kato RM, Chun S, Detterich J, Cui SX, Iyer NP, Lee NG, et al. Phase-Resolved Functional Lung 0.55T MRI Analysis Demonstrates Ventilation-perfusion Defects Driven by Abnormal Perfusion in Patients With Fontan Circulation. In: C59. PICKING UP THE KIDS AT BALBOA PARK: INSIGHTS IN PEDIATRIC PULMONARY HYPERTENSION. American Thoracic Society International Conference Abstracts. Am J Respir Crit Care Med. 2024;209:A6024.
55 Pöhler GH, Klimes F, Voskrebenzev A, Behrendt L, Czerner C, Gutberlet M, et al. Chronic Thromboembolic Pulmonary Hypertension Perioperative Monitoring Using Phase-Resolved Functional Lung (PREFUL)-MRI. J Magn Reson Imaging. 2020;52(2):610–619.
56 Munidasa S, Couch MJ, Rayment JH, Voskrebenzev A, Seethamraju R, Vogel-Claussen J, et al. Free-breathing MRI for monitoring ventilation changes following antibiotic treatment of pulmonary exacerbations in paediatric cystic fibrosis. Eur Respir J. 2021;57(4):2003104.
57 Friedlander Y, Munidasa S, Thakar A, Ragunayakam N, Venegas C, Kjarsgaard M, et al. Phase-Resolved Functional Lung (PREFUL) MRI to Quantify Ventilation: Feasibility and Physiological Relevance in Severe Asthma. Acad Radiol. 2024;31(8):3416–3426.
58 Klimeš F, Voskrebenzev A, Gutberlet M, Kern AL, Behrendt L, Grimm R, et al. 3D phase-resolved functional lung ventilation MR imaging in healthy volunteers and patients with chronic pulmonary disease. Magn Reson Med. 2021;85(2):912–925.
59 Klimeš F, Plummer JW, Willmering MM, Matheson AM, Bdaiwi AS, Gutberlet M, et al. Quantifying spatial and dynamic lung abnormalities with 3D PREFUL FLORET UTE imaging: A feasibility study. Magn Reson Med. 2025. Online ahead of print.
60 Klimeš F, Voskrebenzev A, Gutberlet M, Obert AJ, Pöhler GH, Grimm R, et al. Repeatability of dynamic 3D phase-resolved functional lung (PREFUL) ventilation MR Imaging in patients with chronic obstructive pulmonary disease and healthy volunteers. J Magn Reson Imaging. 2021;54(2):618–629.
61 Klimeš F, Voskrebenzev A, Gutberlet M, Speth M, Grimm R, Dohna M, et al. Effect of CFTR modulator therapy with elexacaftor/tezacaftor/ivacaftor on pulmonary ventilation derived by 3D phase-resolved functional lung MRI in cystic fibrosis patients. Eur Radiol. 2024;34(1):80–89.

Contact

Andreas Voskrebenzev, Ph.D.
Medizinische Hochschule Hannover
Carl-Neuberg-Str. 1
30625 Hannover
Germany
Voskrebenzev.Andreas@mh-hannover.de

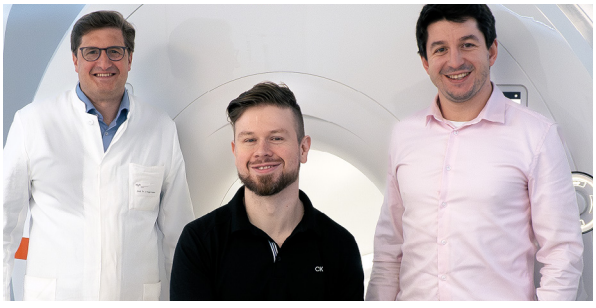

Jens Vogel-Claussen, Andreas Voskrebenzev, Filip Klimeš